P1M.13

ANALYTIC SOLUTION OF THE DEEP CONTINUITY EQUATION OVER COMPLEX TERRAIN

[a]Marco A. Nuñez, [b]Enrique Cruz M.

[a]UNVERSIDAD AUTONOMA METROPOLITANA IZTAPALAPA
[b]UNVERSIDAD AUTONOMA DE LA CIUDAD DE MEXICO

1 Introduction

Several requirements must be met before the credibility of simulations performed with an atmospheric mesoscale model can be established [1]. Among these requirements we have the comparison with known analytic solutions of the equations of motion. In this work we describe a scheme that yields exact solutions of the bidimensional deep continuity equation [1]

$$\boldsymbol{\nabla}\cdot\rho_0(\mathbf{r})\mathbf{U}(\mathbf{r})=0\ . \tag{1}$$

that satisfy the non-flow boundary condition at an arbitrary representation of terrain $h(x)$,

$$\mathbf{U}\cdot\mathbf{n}=0 \quad \text{on} \quad z=h(x), \tag{2}$$

where $\mathbf{n}$ is a vector normal to the lower surface of $z=h(x)$. The exact solutions of the problem (1,2) are useful to study the reliability of a wide class of methods used to estimate a wind field from the data provided by a monitoring network, namely, the so-called mass consistent models [2]. The exact solutions are obtained by means of a suitable modification of the methods provided by complex variable theory (see, e.g., [3,4]).

The primary problem to obtain the velocity field $\mathbf{U}(\mathbf{r})$ is the solution of the so-called shallow continuity equation [1]

$$\boldsymbol{\nabla}\cdot\mathbf{V}(\mathbf{r})=0 \tag{3}$$

under the boundary condition

$$\mathbf{V}\cdot\mathbf{n}=0 \quad \text{on} \quad z=h(x). \tag{4}$$

[0]Corresponding address: [a]Departamento de Fisica, Universidad Autonoma Metropolitana Iztapalapa, A. P. 55-534, Mexico, D. F., C.P. 09340, e-mail: manp@xanum.uam.mx

In fact, let us suppose that $\mathbf{V}$ is known, then it satisfies

$$\boldsymbol{\nabla}\cdot\rho_0(\mathbf{r})\frac{\mathbf{V}(\mathbf{r})}{\rho_0(\mathbf{r})}=0\ .$$

and the boundary condition

$$\frac{\mathbf{V}(\mathbf{r})}{\rho_0(\mathbf{r})}\cdot\mathbf{n}=0 \quad \text{on} \quad z=h(x).$$

Hence the field

$$\mathbf{U}=\frac{\mathbf{V}(\mathbf{r})}{\rho_0(\mathbf{r})}$$

is a solution of equation (1) that satisfies the condition (2). By completeness, in sections 2 and 3 we expose the formal construction of $\mathbf{V}$. Of course, other authors [5] have used complex variable theory to obtain exact solutions of the problem (3,4) but they only consider a computational region with a simple geometry because inherent difficulties of the map-conforming do not permit to solve (3,4) for an arbitrary topography $h(x)$. In section 4 we illustrate the problems posed by the map conforming to obtain solutions of (3,4). These problems can be circumvented if the topography $h(x)$ is estimated by means of *cubic splines* [6], which are defined in section 4. In section 5 we describe the field $\mathbf{V}(\mathbf{r})$ obtained from the natural spline corresponding to real terrain elevation data from the data-base GTOPO30 [7]. It is shown that the map-conforming and the splines generate an exact field $\mathbf{V}$ even when the terrain elevation $h(x)$ changes suddendly as x increases. Histograms of the components of $\mathbf{V}=u\mathbf{i}+w\mathbf{k}$ show that u and w have a very irregular behavior. Similar results are obtained with the components of the field $\mathbf{U}=\rho_0^{-1}\mathbf{V}$ where ρ_0 is the density corresponding to an atmospheric reference state that is isothermic or adiabatic. The field $\mathbf{U}$ is more interesting because its vorticity is not trivial,

$$\nabla\times\mathbf{U}\neq\mathbf{0}\ ,$$

a property that is exhibited by the behavior of the components of $\mathbf{U}$ as a function of the height z.

There is no consensus about the correct representation of the topography in atmospheric models. In general, the terrain data are subject to a smoothing process. Cubic splines can be used to smooth terrain elevation data and, consequently, we can compute the fields $\mathbf{V}$ and $\mathbf{U}$. In section 5 we describe the smoothing splines and the corresponding fields $\mathbf{V}$ and $\mathbf{U}$. The results show that the $\mathbf{V}$ and $\mathbf{U}$ are critically dependent of $h(x)$.

2 Formal construction of the field V

In this section we give a summary of the theory of bidimensional potential flow. Let x, y, z be the a cartesian coordinate system with its origin on a spherical earth model, the z axis out of the sphere and the plane xy is tangent to the sphere at a point with latitude ϕ and longitude λ, the corresponding unit vectors are $\mathbf{i}$, $\mathbf{j}$, $\mathbf{k}$. If the field $\mathbf{V}$ is irrotational,

$$\nabla \times \mathbf{V} = \mathbf{0}$$

there exists a function ϕ (the velocity potential) such that

$$\mathbf{V} = \nabla\phi. \tag{5}$$

If $\mathbf{V}$ satisfies (3) and (4), then ϕ has to satisfy the Laplace equation

$$\nabla^2\phi = 0 \tag{6}$$

and the boundary condition

$$\frac{\partial\phi}{\partial n} \equiv \nabla\phi \cdot \mathbf{n} = 0 \quad \text{on} \quad z = h(x). \tag{7}$$

The velocity field $\mathbf{V}$ can be obtained by solving (6) with the boundary condition (7) without directly using the momentum equation

$$\frac{d\mathbf{V}}{dt} = -\frac{1}{\rho}\nabla p + \mathbf{g}$$

which can be used to obtain the pressure field. A second function can be defined in such a way that the associated velocity field automatically satisfies the equation (3). In fact, the field $\mathbf{V} = \mathbf{i}u + \mathbf{k}w$ with components

$$u = \frac{\partial\psi}{\partial z} \qquad w = -\frac{\partial\psi}{\partial x} \tag{9}$$

satisfies (3) for any function ψ (the stream function). In vectorial form $\mathbf{V}$ is given by

$$\mathbf{V} = \mathbf{j} \times \boldsymbol{\nabla}\psi\ . \tag{10}$$

The irrotational condition $\nabla \times (\mathbf{j} \times \boldsymbol{\nabla}\psi) = \mathbf{0}$ that ψ must satisfy, takes the form $\nabla^2\psi = 0$. The function ψ has useful properties that allow us to obtain the field $\mathbf{V}$ that satisfies (3) and (4) with an arbitrary topography $h(x)$. Let $\mathbf{r}(\eta) = x(\eta)\mathbf{i} + z(\eta)\mathbf{k}$ be the equation of a curve where ψ has a constant value ψ_0,

$$\psi(x(\eta), z(\eta)) = \psi_0,$$

then

$$\boldsymbol{\nabla}\psi \cdot \frac{d\mathbf{r}(\eta)}{d\eta} = 0$$

From (10) we get $\boldsymbol{\nabla}\psi = -\mathbf{j} \times \mathbf{V}$ and replacing in the last equation we have

$$(-\mathbf{j} \times \mathbf{V}) \cdot \frac{d\mathbf{r}(\eta)}{d\eta} = (\mathbf{V} \times \frac{d\mathbf{r}(\eta)}{d\eta}) \cdot \mathbf{j} = \mathbf{0}.$$

Since $\mathbf{V}$ and $\mathbf{r}(\eta)$ belong to the $xz-$plane, it follows that $\mathbf{V}$ is parallel to the vector $d\mathbf{r}/d\eta$; that is, $\mathbf{V}$ is tangent to the curve $\mathbf{r}(\eta)$. Thus we have

$$u = \frac{\partial\psi}{\partial z} = \frac{\partial\phi}{\partial x} \qquad w = -\frac{\partial\psi}{\partial x} = \frac{\partial\phi}{\partial z}\ . \tag{11}$$

The relationships between the derivatives of ψ and ϕ are the so-called Cauchy-Riemann equations, which imply that ψ and ϕ are the components of the function (called the complex potential of $\mathbf{V}$)

$$F(\xi) = \phi(x, z) + i\psi(x, z)$$

of the complex variable

$$\xi = x + iz$$

in terms of which $\mathbf{V}$ is given by

$$\mathbf{V} = V = \frac{dF(\xi)}{d\xi} = u - iw\ . \tag{12}$$

An important property of complex analytic functions to obtain our velocity field $\mathbf{V}$ is that they keep the angle between curves. In fact, let us consider an abstract complex plane

$$\zeta = \bar{x} + i\bar{z}$$

and let

$$\bar{F}(\zeta) = \bar{\phi}(\bar{x}, \bar{z}) + i\bar{\psi}(\bar{x}, \bar{z})$$

be a complex potential so that

$$\bar{V} = \frac{d\bar{F}(\zeta)}{d\zeta} = \bar{u} - i\bar{w}$$

defines a velocity field in the ζ plane with potential $\bar{\phi} = \mathrm{Re}\,\bar{F}(\zeta)$ and stream function $\bar{\psi} = \mathrm{Im}\,\bar{F}(\zeta)$. Let us consider that there is a relationship between ξ and ζ,

$$\xi = G(\zeta),$$

and let us denote the inverse transformation by G^{-1},

$$\zeta = G^{-1}(\xi).$$

The complex potential

$$F(\xi) = \bar{F}[G^{-1}(\xi)] = \phi(x,z) + i\psi(x,z)$$

yields a velocity field V (12) in the $xz-$plane that is the image of $\bar{V}$ under the transformation $G(\zeta)$. Suppose that $G(\zeta)$ is an analytic function of ζ, then G transforms stream lines of the flow $\bar{V}$ in the $\zeta-$plane into stream lines of the field V and analogously with the equipotential lines [4]. Thus, if G transforms a stream line of $\bar{V}$ into the curve $z = h(x)$, the flow V automatically satisfies the continuity equation (3) and the boundary condition (4). In this way, the problem to compute our desired velocity field V consists in defining a field $\bar{V}$ in the $\zeta-$plane with a stream line $\bar{\psi} = \bar{\psi}_0$ whose image under an analytic function $G(\zeta)$ is the curve $z = h(x)$.

Suppose that we know a field $\bar{V}$ and a function $G(\zeta)$ with the aforementioned properties. The desired field V can be obtained from the stream function $\psi(x,y)$ or the potential $\phi(x,y)$ as follows. In principle, from the inverse transformation G^{-1},

$$\zeta = \bar{x} + i\bar{z} = G^{-1}(\xi) = \bar{x}(x,z) + i\bar{z}(x,z) \tag{13a}$$

we get the inverse transformation equations

$$\bar{x} = \bar{x}(x,z), \qquad \bar{z} = \bar{z}(x,z). \tag{13b}$$

The substitution of these expressions in the equation

$$\begin{aligned} F(\xi) &= \bar{F}[G^{-1}(\xi)] \\ &= \phi(x,z) + i\psi(x,z) \\ &= \bar{\phi}(\bar{x},\bar{z}) + i\bar{\psi}(\bar{x},\bar{z}) \end{aligned}$$

yields the relationship between ϕ, ψ and $\bar{\phi}$, $\bar{\psi}$, namely,

$$\begin{aligned} \phi(x,z) &= \bar{\phi}[\bar{x}(x,z), \bar{z}(x,z)] \\ \psi(x,z) &= \bar{\psi}[\bar{x}(x,z), \bar{z}(x,z)] \end{aligned}$$

and, therefore, the desired field V has the components

$$\begin{aligned} u &= \frac{\partial\bar{\psi}}{\partial z} = \frac{\partial\bar{\phi}}{\partial x} \\ w &= -\frac{\partial\bar{\psi}}{\partial x} = \frac{\partial\bar{\phi}}{\partial z}\ . \end{aligned} \tag{14}$$

The chain rule yields the equations

$$\begin{aligned} u &= \frac{\partial\phi}{\partial x} = \frac{\partial\bar{x}}{\partial x}\frac{\partial\bar{\phi}}{\partial\bar{x}} + \frac{\partial\bar{z}}{\partial x}\frac{\partial\bar{\phi}}{\partial\bar{z}} \\ w &= \frac{\partial\phi}{\partial z} = \frac{\partial\bar{x}}{\partial z}\frac{\partial\bar{\phi}}{\partial\bar{x}} + \frac{\partial\bar{z}}{\partial z}\frac{\partial\bar{\phi}}{\partial\bar{z}} \end{aligned}$$

which, in terms of the components $\bar{u}$ and $\bar{w}$ of $\bar{V}$ [eq. (11)], take the form

$$\begin{aligned} u &= \frac{\partial\bar{x}}{\partial x}\bar{u} + \frac{\partial\bar{z}}{\partial x}\bar{w} \\ w &= \frac{\partial\bar{x}}{\partial z}\bar{u} + \frac{\partial\bar{z}}{\partial z}\bar{w}\ . \end{aligned}$$

The coefficients of $\bar{u}$ and $\bar{w}$ are the elements of the matrix

$$\mathbb{J}^{-1} = \begin{pmatrix} \frac{\partial\bar{x}}{\partial x} & \frac{\partial\bar{x}}{\partial z} \\ \frac{\partial\bar{z}}{\partial x} & \frac{\partial\bar{z}}{\partial z} \end{pmatrix}$$

which is the inverse of the Jacobian matrix

$$\mathbb{J} = \begin{pmatrix} \frac{\partial x}{\partial\bar{x}} & \frac{\partial x}{\partial\bar{z}} \\ \frac{\partial z}{\partial\bar{x}} & \frac{\partial z}{\partial\bar{z}} \end{pmatrix}$$

associated to the *direct* transformation equations

$$\begin{aligned} x &= x(\bar{x},\ \bar{z}) = \mathrm{Re}\,G(\zeta) \\ z &= z(\bar{x},\ \bar{z}) = \mathrm{Im}\,G(\zeta) \end{aligned} \tag{15}$$

which are obtained from $\xi = G(\zeta)$. Thus we have

$$\mathbb{J}^{-1} = \begin{pmatrix} \frac{\partial x}{\partial\bar{x}} & \frac{\partial x}{\partial\bar{z}} \\ \frac{\partial z}{\partial\bar{x}} & \frac{\partial z}{\partial\bar{z}} \end{pmatrix}^{-1} = \frac{1}{J}\begin{pmatrix} \frac{\partial z}{\partial\bar{z}} & -\frac{\partial x}{\partial\bar{z}} \\ -\frac{\partial z}{\partial\bar{x}} & \frac{\partial x}{\partial\bar{x}} \end{pmatrix},$$

where $J = \det(\mathbb{J})$,

$$\begin{aligned} \frac{\partial\bar{x}}{\partial x} &= \frac{1}{J}\frac{\partial z}{\partial\bar{z}}, & \frac{\partial\bar{x}}{\partial z} &= -\frac{1}{J}\frac{\partial x}{\partial\bar{z}} \\ \frac{\partial\bar{z}}{\partial x} &= \frac{-1}{J}\frac{\partial z}{\partial\bar{x}}, & \frac{\partial\bar{z}}{\partial z} &= \frac{1}{J}\frac{\partial x}{\partial\bar{x}} \end{aligned}$$

and

$$\begin{pmatrix} u \\ w \end{pmatrix} = \frac{1}{J}\begin{pmatrix} \frac{\partial z}{\partial\bar{z}} & -\frac{\partial z}{\partial\bar{x}} \\ -\frac{\partial x}{\partial\bar{z}} & \frac{\partial x}{\partial\bar{x}} \end{pmatrix}\begin{pmatrix} \bar{u} \\ \bar{w} \end{pmatrix}.$$

The elements of $\mathbb{J}^{-1}$ are not independent, since $G(\zeta) = x(\bar{x},\bar{z}) + iz(\bar{x},\bar{z})$ is analytic the Cauchy-Reimann equations are valid and yield

$$\begin{aligned} \frac{\partial x}{\partial\bar{x}} &= \frac{\partial z}{\partial\bar{z}} \\ \frac{\partial x}{\partial\bar{z}} &= -\frac{\partial z}{\partial\bar{x}}\ . \end{aligned}$$

Thus we get two equivalent expressions to obtain u, w from $\bar{u}$, $\bar{w}$, namely,

$$\begin{aligned} \begin{pmatrix} u \\ w \end{pmatrix} &= \frac{1}{J}\begin{pmatrix} \frac{\partial x}{\partial\bar{x}} & -\frac{\partial z}{\partial\bar{x}} \\ \frac{\partial z}{\partial\bar{x}} & \frac{\partial x}{\partial\bar{x}} \end{pmatrix}\begin{pmatrix} \bar{u} \\ \bar{w} \end{pmatrix} \\ &= \frac{1}{J}\begin{pmatrix} \frac{\partial z}{\partial\bar{z}} & \frac{\partial x}{\partial\bar{z}} \\ -\frac{\partial x}{\partial\bar{z}} & \frac{\partial z}{\partial\bar{z}} \end{pmatrix}\begin{pmatrix} \bar{u} \\ \bar{w} \end{pmatrix}. \end{aligned} \tag{16}$$

3 The case of a uniform flow $\bar{V}$ in the plane ζ

In this section we consider the simplest flow $\bar{V}$ in the complex plane ζ and an analytic function $G(\zeta)$ that transforms a stream line of $\bar{V}$ into a terrain curve $z = h(x)$. The flow in question is the uniform field

$$\bar{V} = V_0 \qquad (\bar{u} = V_0,\ \bar{w} = 0)$$

obtained from the potential

$$\bar{\phi} = V_0 \bar{x}.$$

The corresponding flow V under an *arbitrary* analytic transformation $G(\zeta)$ is [eq. (16)]

$$\begin{aligned} u &= \frac{V_0}{J}\frac{\partial z}{\partial \bar{z}} \qquad (17) \\ w &= -\frac{V_0}{J}\frac{\partial x}{\partial \bar{z}}. \end{aligned}$$

The real axis $\bar{z} = 0$ in the $\zeta-$plane is a stream line of $\bar{V}$, and the simplest function $G(\zeta)$ that transforms such an axis into the curve $z = h(x)$ is

$$G(\zeta) = \zeta + ih(\zeta). \qquad (18)$$

In fact, if ζ is replaced by $\zeta = \bar{x}$ we get

$$G(\zeta) = \bar{x} + ih(\bar{x})$$

which is exactly the parametric form of the curve $z = h(x)$ with $x = \bar{x}$. Let h_1 and h_2 be the real and imaginary parts of $h(\zeta)$,

$$h(\zeta) = h_1(\bar{x},\ \bar{z}) + ih_2(\bar{x},\ \bar{z}),$$

then the transformation equations defined by (15) are

$$\begin{aligned} x &= x(\bar{x},\ \bar{z}) = \bar{x} - h_2(\bar{x},\ \bar{z}) \qquad (19) \\ z &= z(\bar{x},\ \bar{z}) = \bar{z} + h_1(\bar{x},\ \bar{z}). \end{aligned}$$

4 Problems posed by conforming map and splines

In principle any (analytic) representation of the terrain $h(\zeta)$ can be used in the transformation $G(\zeta) = \zeta + ih(\zeta)$. For instance, let us consider the topography

$$h(\zeta) = \sin \pi\zeta/a$$

where a is a positive real number. The corresponding transformation equations (19) are

$$\begin{aligned} x &= x(\bar{x},\ \bar{z}) = \bar{x} - \cos(\pi\bar{x}/a)\ \sinh(\pi\bar{z}/a) \qquad (20) \\ z &= z(\bar{x},\ \bar{z}) = \bar{z} + \sin(\pi\bar{x}/a)\ \cosh(\pi\bar{z}/a). \end{aligned}$$

The presence of the hyperbolic functions implies that a region in the $\zeta-$plane is substantially different in the $\xi-$plane. Figure 1 shows that the image of the semiplane $\{\zeta : \mathrm{Im}\,\zeta \geq 0\}$ under the transformation $\xi = \sin \pi\zeta/a$, is a very small region of the $\xi-$plane (the physical space). This implies that we cannot compute the desired field V on an *arbitrary* region of the physical space. This example also shows the convenience of computing the field V using $\bar{x}$ and $\bar{z}$ as independent variables [eq. (16)], since in general the inverse transformation (13a,b) cannot be obtained in a closed and analytic form because of the nonlinearity of the direct transformation (19) as occurs with (20).

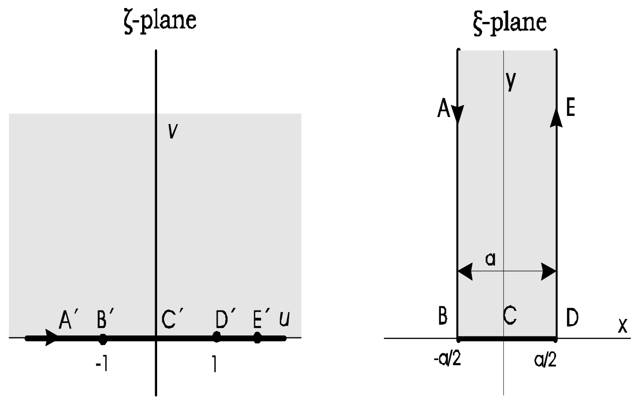

Figure 1: Region in the $\zeta-$plane and its image in the $\xi-$plane with $h(\zeta) = \sin \pi\zeta/a$.

Since our primary objective is the calculation of a velocity field V that satisfies (3) and the boundary condition (4) we can replace an arbitrary (but analytic) topography $h(x)$ by a simpler representation that eliminates the inherent problem of the map conforming. In this section $h(x)$ is approximated by a *natural spline* $S(x)$ which is defined as follows. Let $\{x_k\}_{k=0}^{n}$ be a set of points where the terrain height $h(x_k)$ is known, then : (i) $S(x)$ satisfies

$$S(x_k) = h(x_k) \text{ for } k = 0, ..., n,$$

(ii) $S(x)$ is a cubic polynomial on each interval $[x_k, x_{k+1}]$,

$$\begin{aligned} S(x) &= a_k + b_k(x - x_k) + c_k(x - x_k)^2 + d_k(x - x_k)^3 \\ \text{for } x &\in [x_k, x_{k+1}], \end{aligned}$$

(iii) $S(x)$ and its derivatives $S'(x)$, $S''(x)$ are continuous on $[x_0, x_n]$ and $S''(x)$ satisfies

$$S''(x_0) = S''(x_n) = 0.$$

There is a unique natural spline associated to an analytic function $h(x)$ on the interval $[x_0, x_n]$. Since $S(x)$ is a cubic polynomial on each interval $[x_k, x_{k+1}]$, we can compute the flow

$$\begin{aligned} u &= \frac{V_0}{J}\frac{\partial z^{(k)}}{\partial \bar{z}} \\ w &= -\frac{V_0}{J}\frac{\partial x^{(k)}}{\partial \bar{z}} \quad \text{for } x \in [x_k, x_{k+1}], \end{aligned}$$

where

$$\begin{aligned} x^{(k)} &= \bar{x} - S_2(\bar{x},\ \bar{z}) \\ z^{(k)} &= \bar{z} + S_1(\bar{x},\ \bar{z}) \end{aligned}$$

and

$$S(\zeta = \bar{x} + i\bar{z}) = S_1(\bar{x},\ \bar{z}) + i\ S_2(\bar{x},\ \bar{z}).$$

The continuity of $S(x)$, $S'(x)$ and $S''(x)$ guarantees that the field $\mathbf{V} = u\mathbf{i} + w\mathbf{k}$, its first derivatives

$$\frac{\partial u}{\partial x}, \frac{\partial u}{\partial z}, \frac{\partial w}{\partial x}, \frac{\partial w}{\partial z},$$

and $\nabla \cdot \mathbf{V}$ are continuous on the interval $[x_0, x_n]$. This together with the fact that u, w satisfy the continuity equation (3) and the boundary condition (4) on each interval $[x_k, x_{k+1}]$, implies that the field $\mathbf{V}$ satisfies the same equations on the whole interval $[x_0, x_n]$.

Remark. A clear advantage of the splines is that they can be used to model real terrain elevation data $h(x_k)$ which are known only on a discrete set of points $\{x_k, h(x_k)\}$ which constitute a digital terrain elevation model.

5 Examples

The velocity fields considered below are calculated with the datum $u = 10$ ms^{-1} and $w = 0$ at the point $(x = 0, z = 10$ km), which is used to define the magnitude V_0 of the flow on the abstract complex plane ζ.

5.1 Flow V from a natural spline

In this section we consider the field $\mathbf{V}$ defined by the *natural spline* corresponding to the terrain data $\{x_k, h(x_k)\}$ of fig. 2 with $-400 \leq x \leq 400$ km, the data were obtained from the base GTOPO30 [7]. The field $\mathbf{V}$ is a solution of the shallow continuity equation (3) and the boundary condition (4), with ρ constant, Hereafter, we describe the part of the field on the region $-10 \leq x \leq 10$ km. Figures 3 and 4 show $\mathbf{V}(x, z)$ on lines with $x = x_0 =$ constant

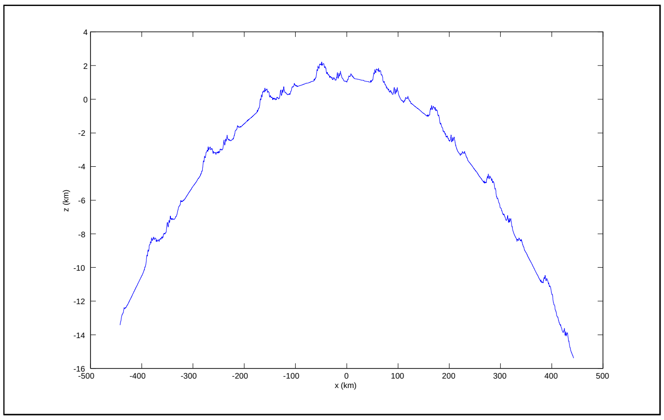

Figure 2: Topography used to compute a natural spline $S(x)$.

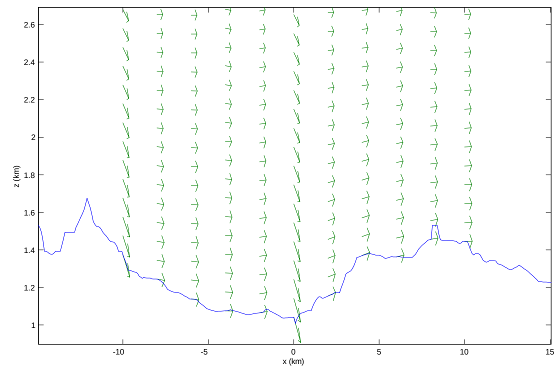

Figure 3: Field $\mathbf{V}(x_0, z)$ at points with x_0 =constant.

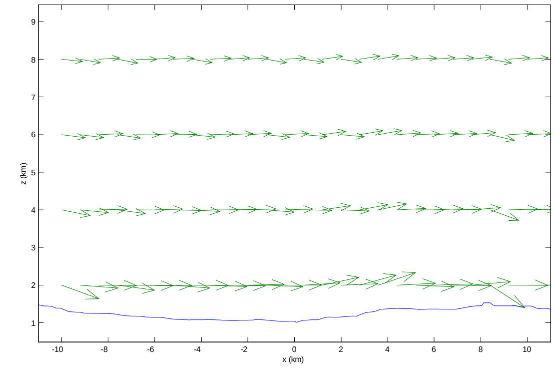

Figure 4: Field $\mathbf{V}(x, z_0)$ at points with z_0 =constant.

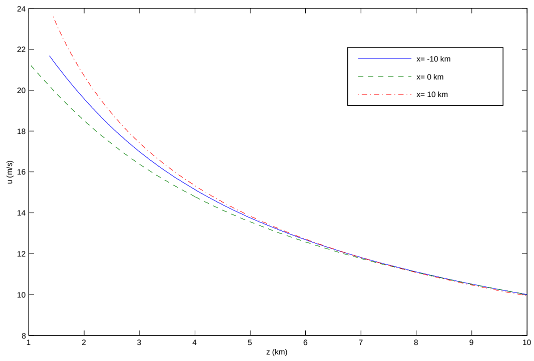

Figure 5: Graph of z v.s. $u\,(x_0, z)$ at $x_0 = -10,\,0,\,10$ km.

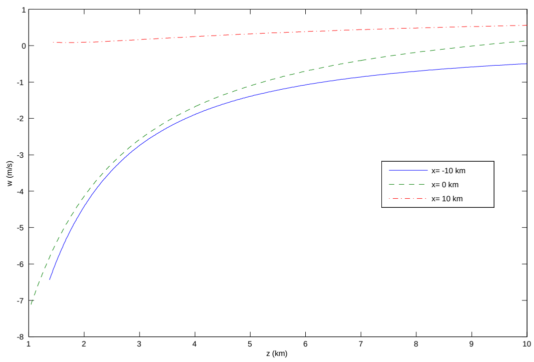

Figure 6: Graph of z v.s. $w\,(x_0, z)$ at $x_0 = -10,\,0,\,10$ km.

and $z = z_0 =$ constant, respectively. Each figure shows the effect of the topography on $\mathbf{V}(x, z)$.

Figures 5 and 6 show the plot of z v.s. $u\,(x_0, z)$ and $w\,(x_0, z)$, respectively, at $x_0 = -10, 0, 10$ km. The graphs allows us to see the continuity of $u\,(x, z)$ and $w\,(x, z)$ as z increases from the topography $z = h(x)$.

Figures 7 and 8 show the plot of x v.s. $u\,(x, z_0)$ and $w\,(x, z_0)$, respectively, at $z_0 = 2$, 10 km. The graphs show that $u\,(x, z)$ and $w\,(x, z)$ have an irregular behavior as x increases, a result that can be attributed to the topography. The case of $w\,(x, z_0 = 2)$ is particularly interesting since we observe that it behaves very irregularly. In principle, the continuity of the spline and its first two derivatives should produce smooth graphs of $u\,(x, z_0)$ and $w\,(x, z_0)$, but the figures 7 and 8 allows us to see that the field $\mathbf{V}\,(x, z)$ keeps the sudden changes of the topography.

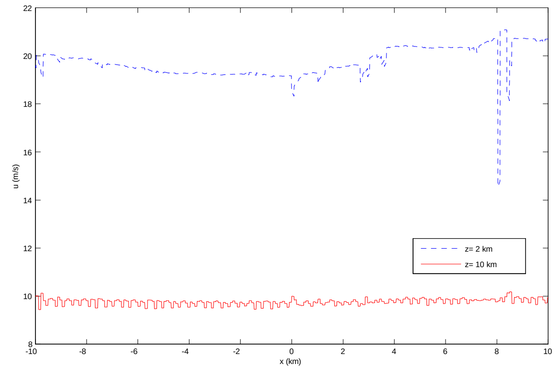

Figure 7: Graph of x v.s. $u\,(x, z_0)$ at $z_0 = 2,\,10$ km.

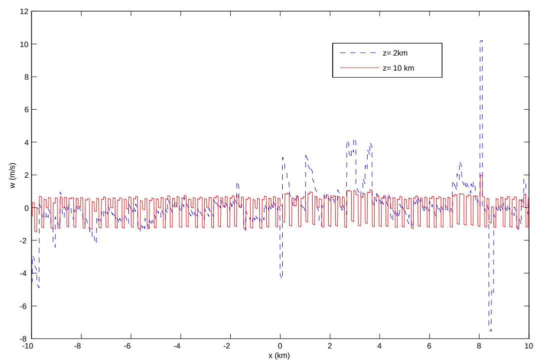

Figure 8: Graph of x v.s. $w\,(x, z_0)$ at $z_0 = 2,\,10$ km.

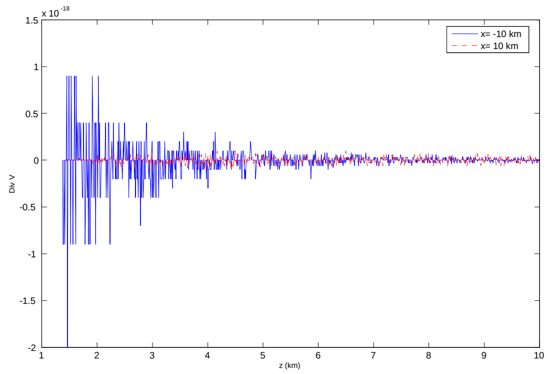

Figure 9: Graph of z v.s. $\boldsymbol{\nabla} \cdot \mathbf{V}\,(x_0, z)$ at $x_0 = -10$, 10 km.

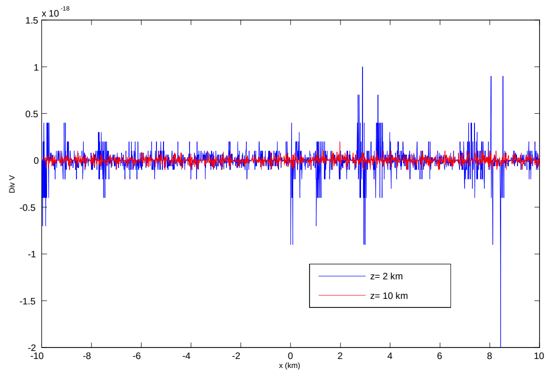

Figure 10: Graph of x v.s. $\boldsymbol{\nabla} \cdot \mathbf{V}\,(x, z_0)$ at $z_0 = 2$, 10 km.

In order to show that the continuity equation $\boldsymbol{\nabla} \cdot \mathbf{V}\,(x, z) = 0$ is satisfied we plot the values $\boldsymbol{\nabla} \cdot \mathbf{V}\,(x, z)$ at points (x_0, z) and (x, z_0) in figures 9 and 10, respectively. As expected, we see that $\boldsymbol{\nabla} \cdot \mathbf{V}\,(x, z)$ is, for practical purposes, zero.

Let us now consider the boundary condition $\mathbf{V} \cdot \mathbf{n} = 0$ on $z = h(x)$. As expected, figure 11 shows that $\mathbf{V} \cdot \mathbf{n}$ is essentially the zero of the computer machine. As above, the irregular behavior is due to the irregularity of the topography.

In order to appreciate the irregular behavior of the components $u\,(x, z_0)$ and $w\,(x, z_0)$ as a function of x with $-10 \leq x \leq 10$, we plotted some histograms. The histrogram of $w\,(x, z_0)$ with $z_0 = 2$ km is plotted in figure 12, and we see that it behaves like a Gaussian distribution with $< w > \sim 0$. Figure 13 shows the histogram of

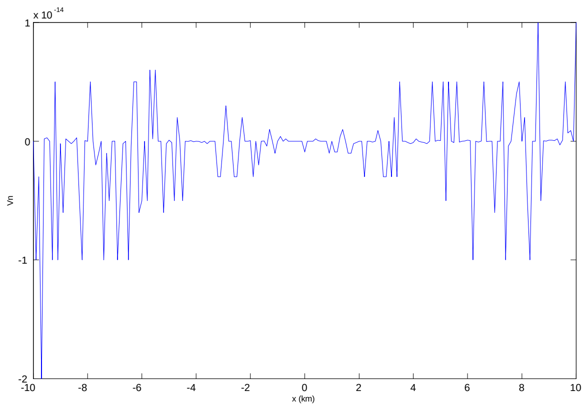

Figure 11: Graph of x v.s. $\mathbf{V} \cdot \mathbf{n}$ at $(x, z = h(x))$.

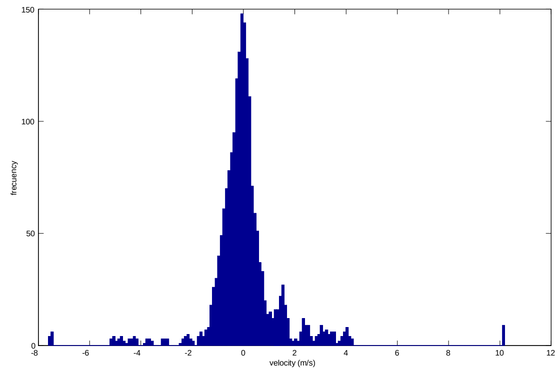

Figure 12: Histogram of $w\,(x, z_0)$ for $-10 \leq x \leq 10$ and $z_0 = 2$ km.

$w\,(x, z_0 = 10$ km$)$, and we see that it behaves like a three-modal distribution. Finally, figures 14 and 15 show the histogram of $u\,(x, z_0)$ at $z_0 = 2$ and 10 km, respectively. The behavior of u at $z_0 = 2$ km is irregular but with a small dispersion, in contrast the behavior at $z_0 = 10$ km is significantly more irregular on a wider range of velocities.

5.2 Flow V from a smoothing spline

In this section we consider the field $\mathbf{V}$ defined by a *smoothing spline* $S_p(x)$ corresponding to the terrain data $\{x_k, h(x_k)\}_{k=1}^{n}$ of fig. 2. The field $\mathbf{V}$ is a solution of the shallow continuity equation (3) and the boundary condition (4), $\rho =$ constant, and we describe the part of the field on the region $-10 \leq x \leq 10$ km. The splines $S_p(x)$

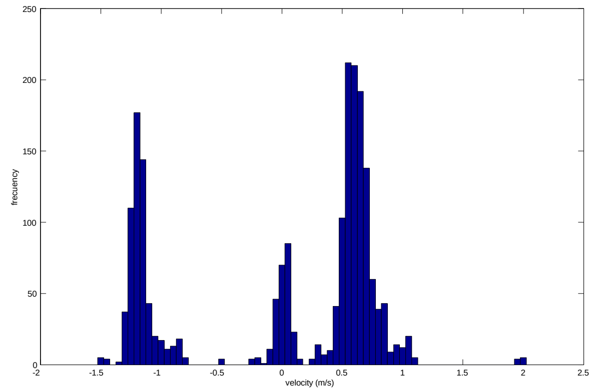

Figure 13: Histogram of $w\,(x, z_0)$ for $-10 \leq x \leq 10$ and $z_0 = 10$ km.

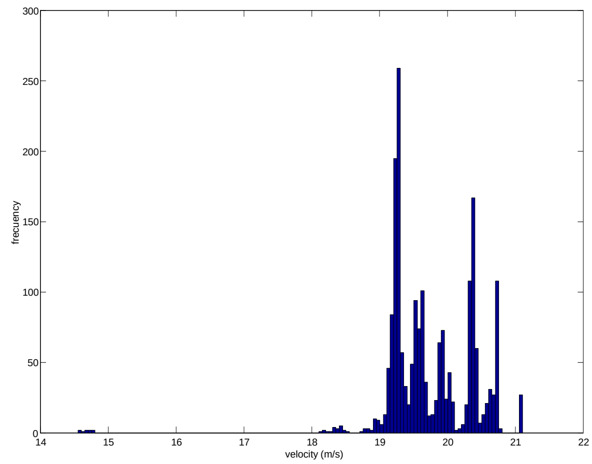

Figure 14: Histogram of $u\,(x, z_0)$ for $-10 \leq x \leq 10$ and $z_0 = 2$ km.

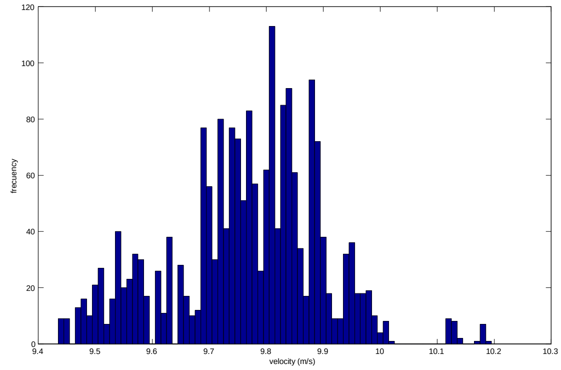

Figure 15: Histogram of $u\,(x, z_0)$ for $-10 \leq x \leq 10$ and $z_0 = 2$ km.

are obtained by minimizing the functional

$$F = p \sum_{k=1}^{n} |h_k - S_p(x_k)|^2 + (1-p) \int_{x_1}^{x_n} |D^2 S_p(t)|^2 dt$$

Here, n is the number of terrain data and the integral is over the smallest interval containing all the data x_k. Further, $D^2 S_p(t)$ denotes the second derivative of $S_p(x)$. The smoothing parameter is p, it determines the relative weight on the contradictory demands of having be smooth v.s. having be close to the data. For $p = 0$, we get the least-squares straight line fit to the data, while, at the other extreme, $p = 1$ yields the *natural* spline. As p moves from 0 to 1, the smoothing spline changes from one extreme to the other.

We begin with the field $\mathbf{V}_{p=0.1}(x, z)$ from the smoother spline $S_p(t)$ with $p = 0.1$. Figures 16 and 17 show $\mathbf{V}_{p=0.1}(x, z)$ on lines with $x = x_0 =$ constant and $z = z_0 =$ constant, respectively. Figures 18 and 19 show the plot of z v.s. $u\,(x_0, z)$ and $w\,(x_0, z)$, respectively, at $x_0 = -10$, 0, 10 km, where we see the continuity of $u\,(x, z)$ and $w\,(x, z)$ as z increases from the topography $z = h(x)$. Figures 20, 21 show the plot of x v.s. $u\,(x, z_0)$ and $w\,(x, z_0)$, respectively, at $z_0 = 2$, 10 km. As expected, u and w are smooth at $z_0 = 2$ km but they become irregular as z_0 increases. The irregularity can be seen in the histograms plotted in figs. 22 to 25.

Figures 26 to 31 show the behavior of $\mathbf{V}_{p=0.5}(x, z)$ from the smoothing spline $S_p(t)$ with $p = 0.5$. Figures 26 and 27 show $\mathbf{V}_{p=0.5}(x, z)$ on lines with $x = x_0$ and $z = z_0$, respectively. Figures 28 and 29 show the plot of z v.s. $u\,(x_0, z)$ and $w\,(x_0, z)$, respectively, at $x_0 = -10$, 0, 10

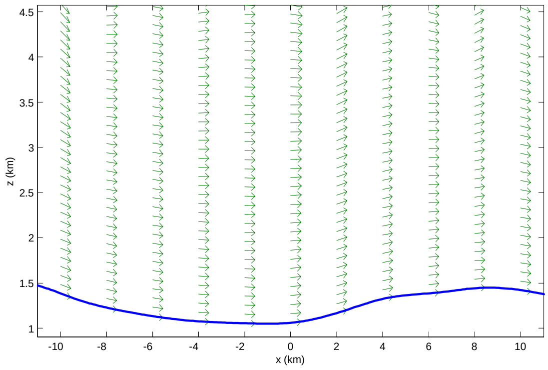

Figure 16: Field $\mathbf{V}_{p=0.1}(x_0, z)$ at points with x_0 =constant.

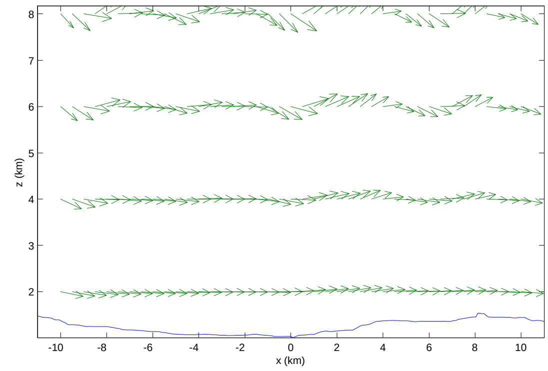

Figure 17: Field $\mathbf{V}_{p=0.1}(x, z_0)$ at points with z_0 =constant.

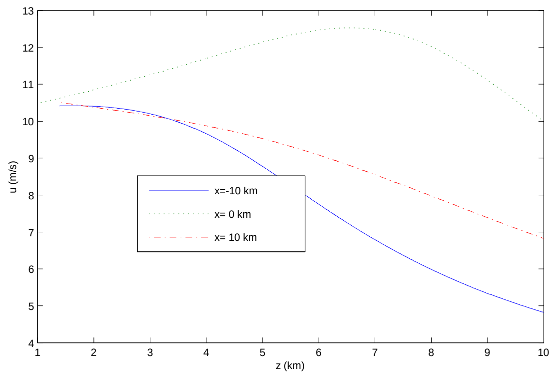

Figure 18: Graph of z v.s. $u_{p=0.1}\,(x_0, z)$ at $x_0 = -10$, 0, 10 km.

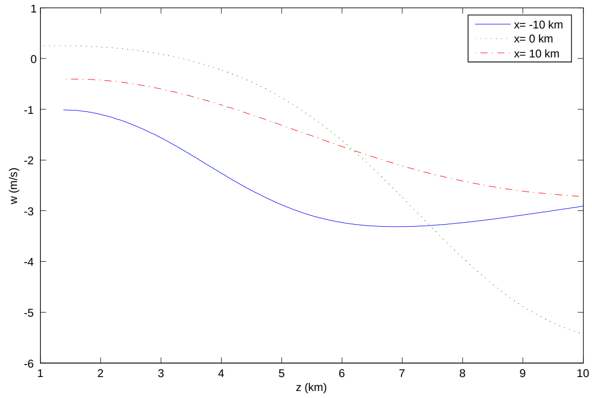

Figure 19: Graph of z v.s. $w_{p=0.1}\,(x_0, z)$ at $x_0 = -10$, 0, 10 km.

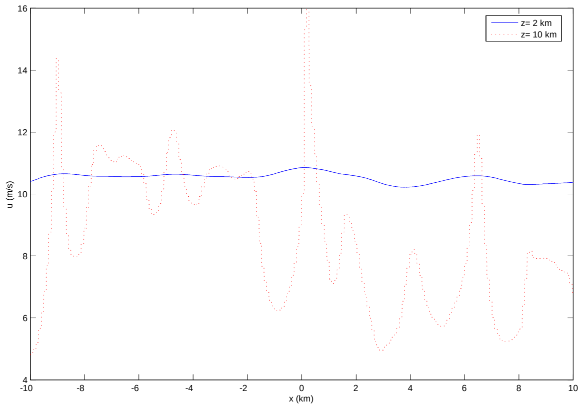

Figure 20: Graph of x v.s. $w_{p=0.1}\,(x, z_0)$ at $z_0 = 2$, 10 km.

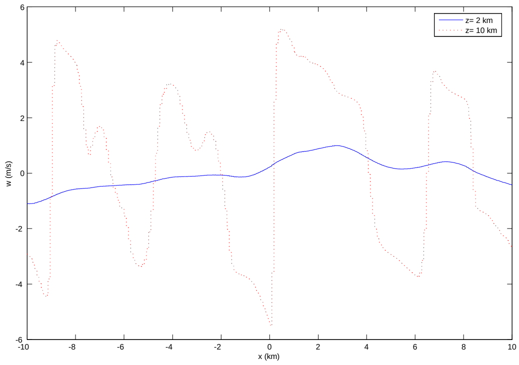

Figure 21: Graph of x v.s. $w_{p=0.1}\left(x,z_0\right)$ at $z_0 = 2,\ 10$ km.

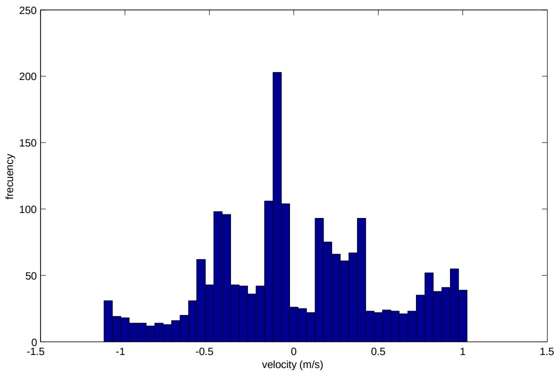

Figure 22: Histogram of $w_{p=0.1}\left(x,z_0\right)$ for $-10 \leq x \leq 10$ and $z_0 = 2$ km.

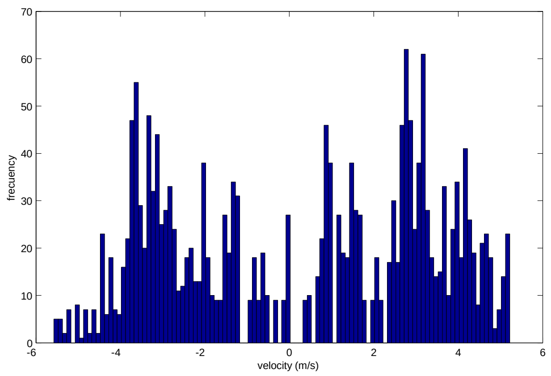

Figure 23: Histogram of $w_{p=0.1}\left(x,z_0\right)$ for $-10 \leq x \leq 10$ and $z_0 = 10$ km.

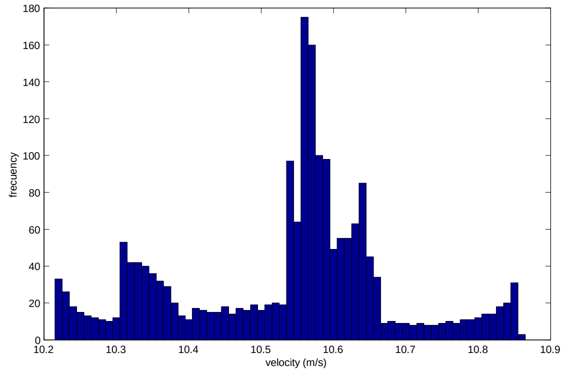

Figure 24: Histogram of $u_{p=0.1}\left(x,z_0\right)$ for $-10 \leq x \leq 10$ and $z_0 = 2$ km.

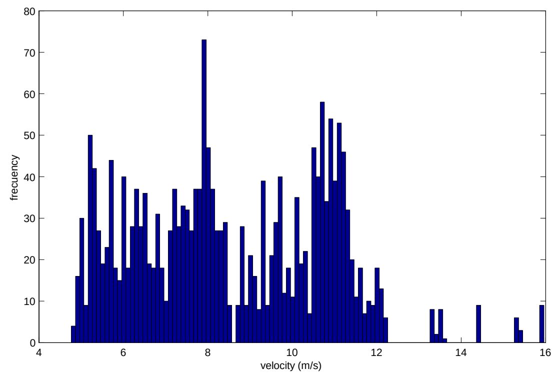

Figure 25: Histogram of $u_{p=0.1}\left(x,z_0\right)$ for $-10 \leq x \leq 10$ and $z_0 = 2$ km.

km, where we see the continuity of $u\,(x,z)$ and $w\,(x,z)$ as z increases from $z=h(x)$. Figures 30, 31 show the plot of x v.s. $u\,(x,z_0)$ and $w\,(x,z_0)$, respectively, at $z_0=2$, 10 km. Once again, u and w are smooth at $z_0=2$ km but they become irregular as z_0 increases.

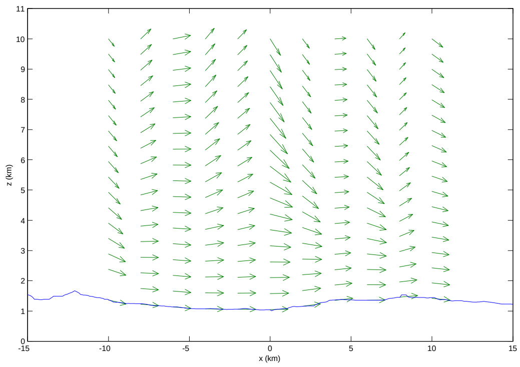

Figure 26: Field $\mathbf{V}_{p=0.5}(x_0,z)$ at points with $x_0=$constant.

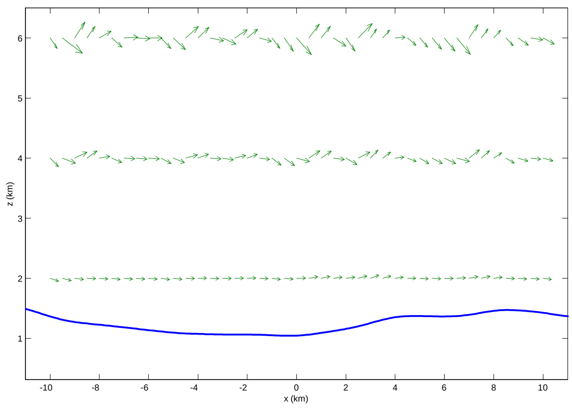

Figure 27: Field $\mathbf{V}_{p=0.5}(x,z_0)$ at points with $z_0=$constant.

Figures 32 to 39 show the behavior of $\mathbf{V}_{p=0.9}(x,z)$ from the smoothing spline $S_p(t)$ with $p=0.9$. Figures 32 and 33 show $\mathbf{V}_{p=0.9}(x,z)$ on lines with $x=x_0$ and $z=z_0$, respectively. Figures 34 and 35 show the plot of z v.s. $u\,(x_0,z)$ and $w\,(x_0,z)$, respectively, at $x_0=-10$, 0, 10 km, where we see the continuity of $u\,(x,z)$ and $w\,(x,z)$ as z increases from $z=h(x)$. The irregularity can be seen in the histograms plotted in figs. 36 to 39.

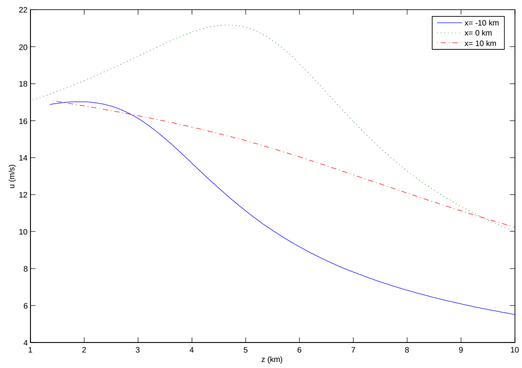

Figure 28: Graph of z v.s. $u_{p=0.1}\,(x_0,z)$ at $x_0=-10$, 0, 10 km.

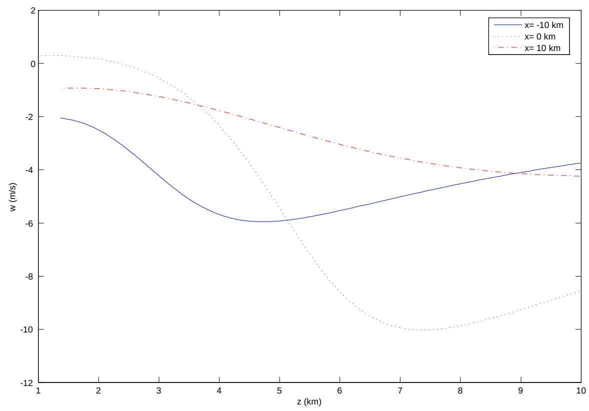

Figure 29: Graph of z v.s. $w_{p=0.5}\,(x_0,z)$ at $x_0=-10$, 0, 10 km.

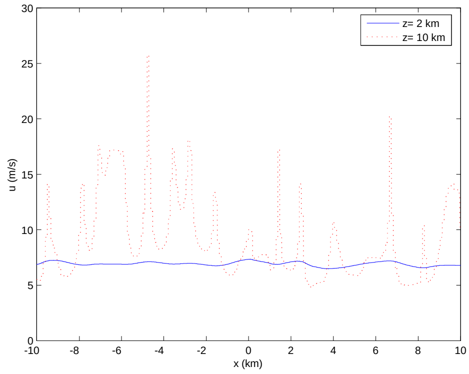

Figure 30: Graph of x v.s. $w_{p=0.5}\,(x, z_0)$ at $z_0\,=\,2,\,10$ km.

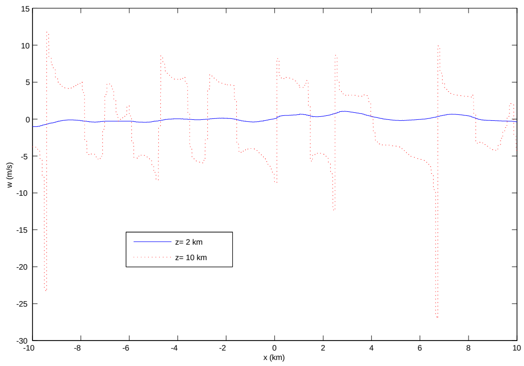

Figure 31: Graph of x v.s. $w_{p=0.5}\,(x, z_0)$ at $z_0\,=\,2,\,10$ km.

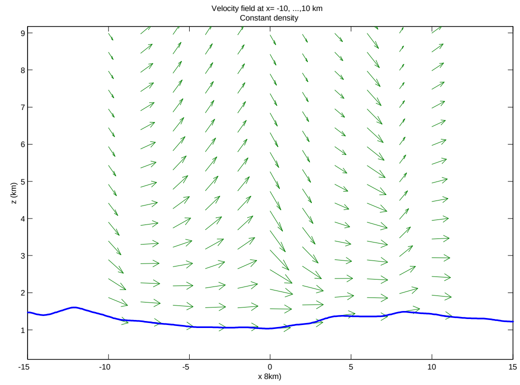

Figure 32: Field $\mathbf{V}_{p=0.9}(x_0, z)$ at points with x_0 =constant.

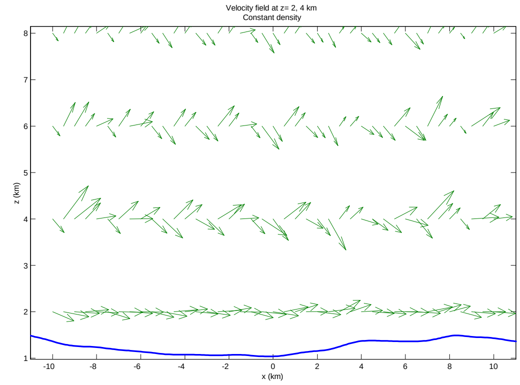

Figure 33: Field $\mathbf{V}_{p=0.9}(x, z_0)$ at points with z_0 =constant.

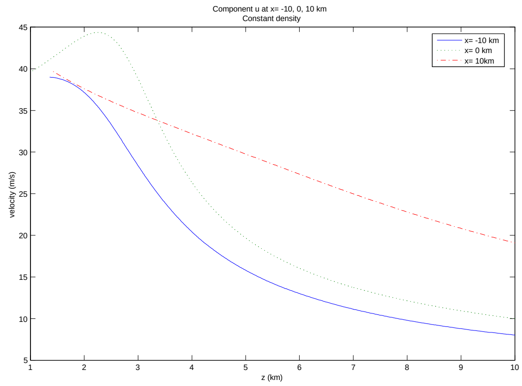

Figure 34: **FIG 34** Graph of z v.s. $u_{p=0.9}\,(x_0, z)$ at $x_0 = -10,\,0,\,10$ km.

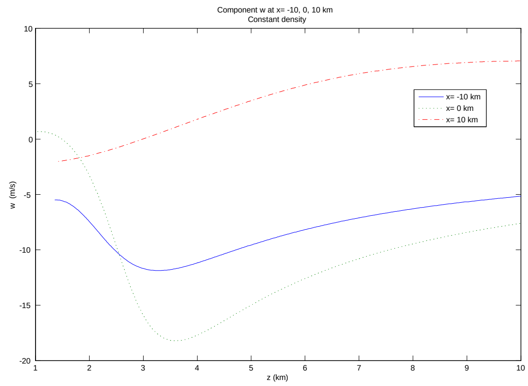

Figure 35: Graph of z v.s. $w_{p=0.9}\,(x_0, z)$ at $x_0 = -10$, 0, 10 km.

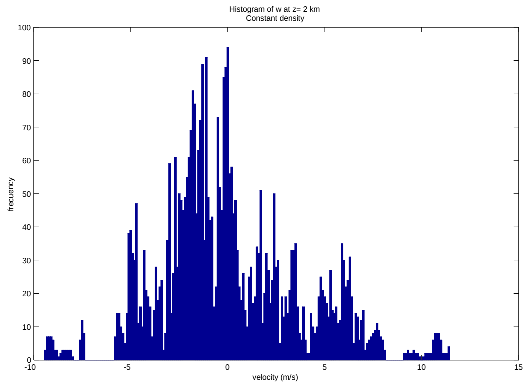

Figure 36: Histogram of $w_{p=0.9}(x, z_0)$ for $-10 \le x \le 10$ and $z_0 = 2$ km.

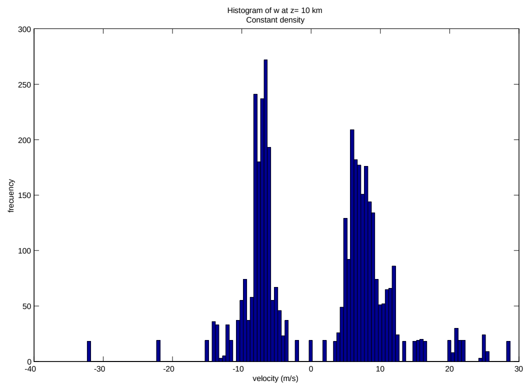

Figure 37: Histogram of $w_{p=0.9}(x, z_0)$ for $-10 \le x \le 10$ and $z_0 = 10$ km.

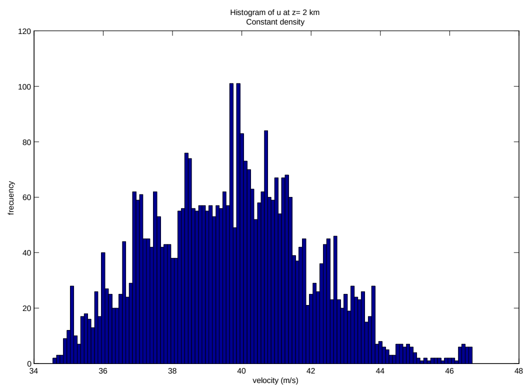

Figure 38: Histogram of $u_{p=0.9}(x, z_0)$ for $-10 \le x \le 10$ and $z_0 = 2$ km.

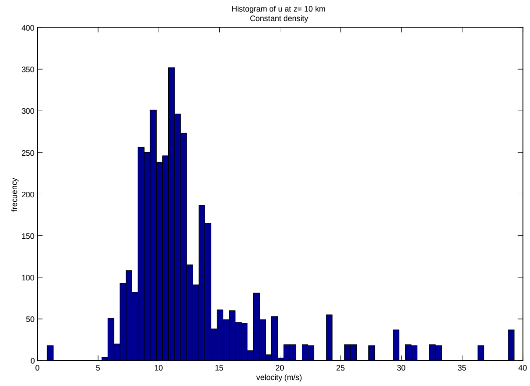

Figure 39: Histogram of $u_{p=0.9}(x, z_0)$ for $-10 \le x \le 10$ and $z_0 = 10$ km.

Figure 40 shows the fields $\mathbf{V}_p$ with $p = 0.1, 0.5, 0.9, 1.0$ where $p = 1$ corresponds to the natural spline. A comparison of the above results shows that "small" changes on the topography (approximated by a spline) produce significant changes in the field $\mathbf{V}_{p=0.5}$. This is particularly evident from the histograms. The most irregular field is $\mathbf{V}_{p=1.0}$. In principle we can expect that $\mathbf{V}_p$ tends to $\mathbf{V}_{p=1.0}$ as $p \to 1.0^-$ but this limiting process is not continuous since the natural spline $S_{p=1}(x)$ is almost discontinuous (see fig. 2).

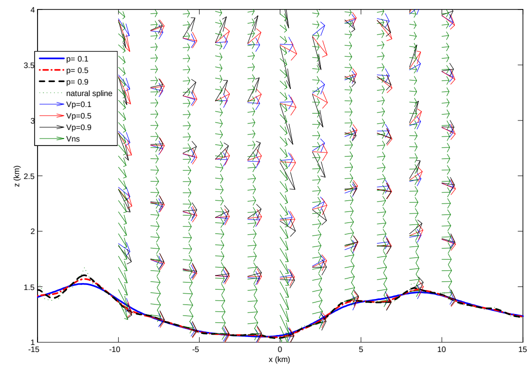

Figure 40: Splines $S_p(x)$ and the corresponding velocity fields $\mathbf{V}_p$ for $p = 0.1, 0.5, 0.9, 1.0$.

Acknowledgments

One of us (M.A.N.) wishes to thank Ma. T. Nuñez by her its invaluable support.

6 References

1. Pielke R. A., *Mesoscale Meteorological Modeling* (Academic Press, New York); 2nd ed (2002)

2. C. F. Ratto, R. Festa, C. Romeo, O. A. Frumento and M. Galluzzi, *Environ. Software* **9**, 247-268 (1994). D. P. Lalas and C. F. Ratto editors, *Modeling of atmospheric fields* (World Scientific, Singapore, 1996)

3. L.D. Landau and E.M. Lifshitz, *Fluid Mechanics* (Pergamon Press, 1987).

4. M. R. Spiegel, *Complex Variable* (McGraw-Hill, 1971).

5. D. G. Ross, I. N. Smith, P. C. Manins and D. G. Fox, *J. Applied Met.* **27**, 675-686 (1988).

6. See, e.g., R. L. Burden and J. D. Fires, Numerical Analysis (Brook/Cole, 2001).

7. GTOPO30 documentation, section 7, U. S. Geological Survey (1997). http:// www.scd.ucar.edu/ dss/datasests/ds758.0hmtl.